Robotica (2011) volume 29, pp. 883–893. © Cambridge University Press 2011
doi:10.1017/S0263574711000099

A novel dynamic walker with heel, ankle, and toe rocker motions

R. Prasanth Kumar†, Abdullah Özer†, Gabsoon Kim‡ and Jungwon Yoon†*

† *School of Mechanical and Aerospace Engineering and ReCAPT, Gyeongsang National University, Jinju, South Korea*
‡ *Department of Control Instrumentation Engineering, Gyeongsang National University, Jinju, South Korea*

(Received in Final Form: January 29, 2011. First published online: March 4, 2011)

SUMMARY

This paper proposes a novel dynamic walker capable of walking with heel, ankle, and toe rocker motions. The heel and toe rocker motions are obtained by using inelastic stoppers between leg and foot, which limit the range of rotation of the foot about the ankle joint. A generalized set of equations of motion and associated transition equations applicable for multiple foot segments is derived. Passive dynamic walking is studied with equal heel and toe strike angles for the case of symmetric foot walking. It is shown that by including the ankle joint, low-speed walking is made possible. The energy efficiency of the proposed walker is studied theoretically and through numerical simulations. Finally, three different underactuated modes of active walking that do not require toe and heel actuation are presented. In order to implement these modes of walking, the proposed walker can be constructed with little modification from an existing flat-foot walker that uses ankle rocker motion alone. Results show that substantial benefits can be obtained in efficiency and stability compared to point/flat-foot walker of the same leg length and mass distribution.

KEYWORDS: Bipeds; Human biomechanics; Humanoid robots; Legged robots; Robot dynamics.

1. Introduction

Passive dynamic walking has been regarded as an approach for highly efficient biped locomotion since McGeer's initial work on passive dynamic walkers.[1] Very low energy consumption and inherent gait stability because of passivity property are the chief features of such biped walkers. Goswami *et al.*[2] extended the passivity property to active dynamic walkers on level ground by proposing energy-based passivity-mimicking control laws. One remarkable feature of such active control is that it does not require trajectory tracking. The zero moment point (ZMP), a critical issue in active biped robots that use trajectory tracking controllers, is autonomously regulated by the control law to yield a stable gait.

Most of the passive dynamic walkers studied till date have either arc-shaped feet or point feet. Their corresponding active dynamic walkers have arc feet with hip actuation or flat feet with ankle and hip actuation. Though arc feet walkers are better than flat-feet walkers in terms of speed and energy efficiency, flat-feet walkers have advantages like the ability to stand still, robustness to floor irregularities, higher floor contact area, etc.[3,4] Apart from these advantages, similarity of appearance of flat foot with human foot is another motivating factor for study.

Mechanical energy balance approach and restoring the mechanical energy lost during heel strike collisions can usually be valuable for supplying the necessary conditions for stable and efficient dynamic gait generation in biped robots. In a recent study with regard to efficiency, it has been shown that sustainable gait generation based on parametric excitation can be obtained via increasing the total mechanical energy of a biped robot with semicircular feet through knee joint actuations.[5,6] Biomechanical studies of humans also indicate that rolling-like motion of human foot reduces the metabolic cost.[7] There have been some studies that address passive dynamic walking with flat feet that have toe and heel rocker motions to create rolling-like motion.[8–10] These studies are limited to passive dynamic walking on a slope using flat feet with rigid ankle. A recent study on limit cycle walkers with flat feet and ankle joint stiffness shows that both efficiency and stability can be improved significantly.[11] By adding ankle joints and inelastic stoppers with locking mechanisms that limit the range of rotation of the feet about the ankle joints, range of walking speed, stability of the walker, and energy efficiency at low speed can be increased,[12] as well as several cases of underactuation during active walking are made possible. Our main motivation in this paper is to derive a generalized set of equations of motion and their associated transition equations for a generalized walker with multiple foot segments connected by joints, and study the characteristics with respect to the number of foot segments. We show that flat foot is a discretization of arc foot and increasing the number of foot segments has the effect of reducing the energy losses because of impacts occurring within the foot because of the presence of segments and joint angle limiting stoppers.

Another motivation for studying the proposed walker is the possibility of underactuated active walking (during toe and heel rocker phases) without using toe and heel actuators. The proposed model in this mode of actuation has higher efficiency and stability though it has the same (or even less) number of actuators as the existing flat-foot walkers. Three cases of underactuated walking are studied to show the feasibility of underactuated walking and its benefits. This

* Corresponding author. Email: jwyoon@gnu.ac.kr

https://doi.org/10.1017/S0263574711000099 Published online by Cambridge University Press

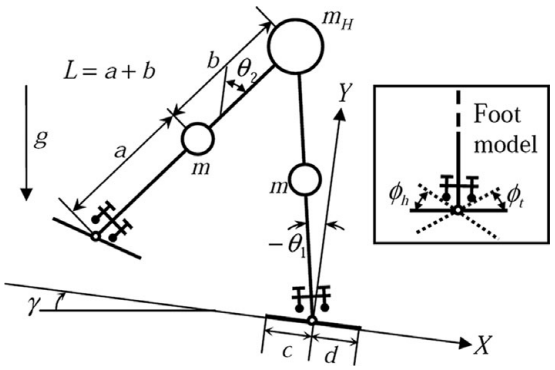


Fig. 1. Proposed biped model in AR phase.

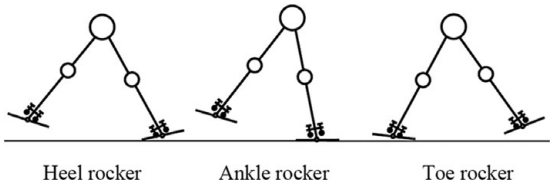


Fig. 2. Heel, ankle, and toe rocker phases of walking.

includes walking with hip alone actuation found in arc-foot walker, which is not possible in flat-foot walkers that uses ankle rocker (AR) alone.[13]

This paper is organized as follows. Section 2 describes the mathematical model of the proposed dynamic walker through generalized equations of motion and generalized transition equations for the heel, ankle, and toe rocker phases so that the equations are applicable to any number of segments in the foot. Section 3 presents a study of passive dynamic walking of the proposed walker. Section 4 discusses the losses during walking because of impacts within the foot and heel strike. Finally, various cases of underactuated walking on level ground without using toe and heel actuators are presented in Section 5, followed by Conclusions. Throughout this paper, we limit our study to period one gait.

2. Model of the Dynamic Walker

The proposed model of the passive dynamic walker along with the notation is shown in Fig. 1. The model is similar to the popular flat-foot walker that uses AR motion alone. However, in order to allow heel and toe rocker motions, inelastic stops are used that limit the range of rotation of the foot about the ankle joint.

The model operates in three consecutive phases for each step, namely, heel rocker, ankle rocker, and toe rocker as shown in Fig. 2. Throughout this paper we use Heel–Ankle–Toe Rocker (HATR) walker to denote the proposed walker, and ankle rocker walker to denote the existing flat-foot or point-foot walkers. The equations of motion for all the three phases and the transition equations between the phases are detailed in the following subsections. These equations are general and applicable to walkers with multiple toe and heel joints in series.

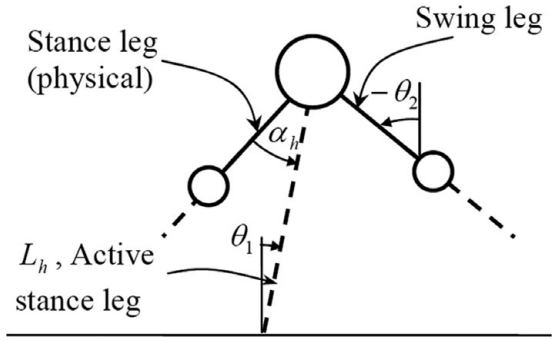


Fig. 3. General rocker motion.

2.1. Equations of motion

Let the generalized equation of motion of the biped (during any of the phases) on a slope of γ be

$$\boldsymbol{M}(\boldsymbol{\theta})\ddot{\boldsymbol{\theta}} + \boldsymbol{C}(\boldsymbol{\theta}, \dot{\boldsymbol{\theta}})\dot{\boldsymbol{\theta}} + \boldsymbol{g}(\boldsymbol{\theta}; \boldsymbol{\gamma}) = \boldsymbol{\tau}, \tag{1}$$

where the control input is zero for passive dynamic walking, $\boldsymbol{\theta} = [\boldsymbol{\theta_1} \quad \boldsymbol{\theta_2}]^T$, $\boldsymbol{\theta_2}$ is the swing leg angle, and θ_1 is the active (either virtual or physical) stance leg angle. Active or effective stance leg is defined as the line joining the hip joint and the ankle joint during AR phase (physical stance leg), or the line joining the hip joint and toe or heel joint during toe or heel rocker phases (virtual stance leg), respectively.

Let m be the mass of each leg and m_H be the hip mass. The inertia and Coriolis/centrifugal terms are, respectively,

$$\boldsymbol{M}(\boldsymbol{\theta}) = \begin{bmatrix} m_{11} & m_{12} \\ m_{21} & m_{22} \end{bmatrix}, \quad \boldsymbol{C}(\boldsymbol{\theta}, \dot{\boldsymbol{\theta}}) = \begin{bmatrix} c_{11} & c_{12} \\ c_{21} & c_{22} \end{bmatrix}.$$

Let L_H be the length of the active stance leg and α_h be the angle between the active stance leg and the physical stance leg as shown in Fig. 3. The angle α_h is constant during each phase of motion, and its value is determined by the length(s) of segment(s) between the active stance leg and the physical stance leg, and the stopper limiting angles at the joint(s) in-between. This angle is negative for heel rocker, positive for toe rocker, and zero for ankle rocker since the active and the physical stance legs coincide. Then,

$$m_{11} = m\left(2L_h^2 + b^2 - 2bL_h\cos\alpha_h\right) + m_h L_h^2, \quad m_{22} = mb^2,$$
$$m_{12} = m_{21} = -mbL_h\cos(\theta_1 - \theta_2),$$
$$c_{11} = c_{22} = 0, \quad c_{12} = -mbL_h\dot{\theta}_2\sin(\theta_1 - \theta_2),$$
$$c_{21} = mbL_h\dot{\theta}_1\sin(\theta_1 - \theta_2),$$

$$g(\boldsymbol{\theta}; \gamma) = \begin{bmatrix} -2mgL_h\sin(\theta_1+\gamma) - m_H L_h\sin(\theta_1+\gamma) + mgb\sin(\alpha_h+\theta_1+\gamma) \\ mgb\sin(\theta_2+\gamma) \end{bmatrix}.$$

https://doi.org/10.1017/S0263574711000099 Published online by Cambridge University Press

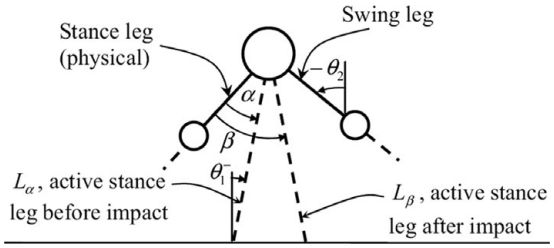


Fig. 4. General impact within the foot.

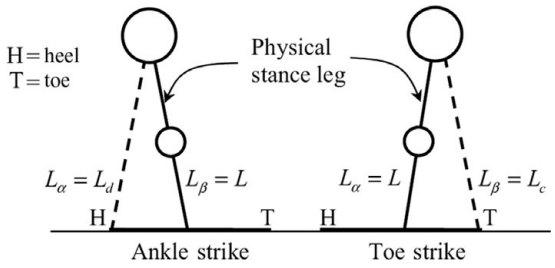


Fig. 5. Impacts within the foot for the simplest foot.

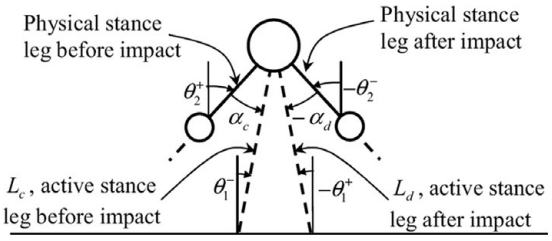


Fig. 6. General heel strike.

2.2. *Transition equations*

The impact transitions between the phases are assumed to be inelastic. The transition equation is given by

$$\boldsymbol{Q}_p\dot{\boldsymbol{\theta}}^+ = \boldsymbol{Q}_m\dot{\boldsymbol{\theta}}^-, \tag{2}$$

where

$$\boldsymbol{Q}_m = \begin{bmatrix} q_{11}^- & q_{12}^- \\ q_{21}^- & q_{22}^- \end{bmatrix}, \quad \boldsymbol{Q}_p = \begin{bmatrix} q_{11}^+ & q_{12}^+ \\ q_{21}^+ & q_{22}^+ \end{bmatrix}, \tag{3}$$

and $\dot{\boldsymbol{\theta}}^-$ and $\dot{\boldsymbol{\theta}}^+$ are leg angle vectors before and after the impact, respectively. The elements of these matrices for various situations are given as follows.

2.2.1. Generalized transition equation for impacts within the foot. Impact is said to occur within the foot when the physical stance leg before impact is same as the physical stance leg after the impact. Let α and β be the angles between the physical stance leg and the active stance leg before and after the impact, respectively, as shown in Fig. 4. These angles are positive when the active stance leg is in front of the physical stance leg as shown in Fig. 4.

Let L_α and L_β represent the lengths of effective stance legs before and after impact, respectively. The elements of the generalized transition equation for impacts within the foot are given by the following:

$$\begin{aligned}
q_{11}^- &= (2m + m_H)L_\alpha L_\beta \cos(\alpha - \beta) + mb(b - L_\beta \cos\beta) \\
&\quad -mbL_\alpha(\cos\alpha + \cos(\theta_1^- - \theta_2^-)), \\
q_{12}^- &= mb(b - L_\beta \cos(\theta_1^- - \theta_2^- + \alpha - \beta)), \\
q_{21}^- &= mbL_\alpha \cos(\theta_1^- - \theta_2^-), \quad q_{22}^- = mb^2, \\
q_{11}^+ &= (2m + m_H)L_\beta^2 + mb^2 \\
&\quad -mbL_\beta(2\cos\beta + \cos(\theta_1^+ - \theta_2^+)), \\
q_{12}^+ &= mb(b - L_\beta \cos(\theta_1^+ - \theta_2^+)), \\
q_{21}^+ &= -mbL_\beta \cos(\theta_1^+ - \theta_2^+), \\
q_{22}^+ &= mb^2, \\
\theta_1^+ &= \theta_1^- + \alpha - \beta, \text{and } \theta_2^+ = \theta_2^-.
\end{aligned} \tag{4}$$

In the case of the simplest foot with one toe segment and one heel segment, let L_c and L_d be the lengths of virtual stance legs during toe and heel rocker phases, respectively. Then, as shown in Fig. 5, for ankle strike

$$L_\alpha = L_d, \quad L_\beta = L, \tag{5}$$

and for toe strike

$$L_\alpha = L, \quad L_\beta = L_c. \tag{6}$$

For a foot with two toe segments and two heel segments, let L_{c1} and L_{c2} be the lengths of virtual stance legs during the toe rocker phases, and L_{d1} and L_{d2} be the lengths of virtual stance legs during the heel rocker phases. The leg lengths are numbered starting from physical leg. For instance, L_{c1} is nearer to the physical stance leg than L_{c2}. Then, for heel strike 1

$$L_\alpha = L_{d2}, \quad L_\beta = L_{d1}, \tag{7}$$

for ankle strike

$$L_\alpha = L_{d1}, \quad L_\beta = L, \tag{8}$$

for toe strike 1

$$L_\alpha = L, \quad L_\beta = L_{c1}, \tag{9}$$

and for toe strike 2

$$L_\alpha = L_{c1}, \quad L_\beta = L_{c2}. \tag{10}$$

2.2.2. Heel strike impact outside the foot. Heel strike impact outside the foot is said to occur when the physical stance leg before the impact is not the same as the physical stance leg after the impact. As shown in Fig. 6, let α_c (positive) be the angle between the physical stance leg and the virtual stance leg L_c during toe rocker just prior to heel strike, and α_d (negative) be the angle between the physical stance leg and the virtual stance leg L_d during heel rocker just after heel

https://doi.org/10.1017/S0263574711000099 Published online by Cambridge University Press

Table I. Physical parameters of the walker.

m_H	10.0 kg
m	5.0 kg
a	0.5 m
b	0.5 m
$L(=a+b)$	1.0 m
$c(=d)$	0.1 m

strike. Then,

$$\begin{aligned}
&\theta_1^+ = \theta_1^- - \alpha_d, \quad \theta_2^+ = \theta_1^- + \alpha_c.\\
&q_{11}^- = (2m + m_H)L_c L_d \cos(\theta_1^- - \theta_2^- + \alpha_d) + mb^2\\
&\qquad -mbL_c(\cos(\theta_1^- - \theta_2^-) + \cos\alpha_c)\\
&\qquad -mbL_d \cos(\theta_1^- - \theta_2^- + \alpha_c + \alpha_d),\\
&q_{12}^- = mb(b - L_d \cos\alpha_d),\\
&q_{21}^- = mb(b - L_c \cos\alpha_c), \quad q_{22}^- = 0,\\
&q_{11}^+ = (2m + m_H)L_d^2 + mb^2\\
&\qquad -mbL_d(2\cos\alpha_c + \cos(\theta_1^+ - \theta_2^+)),\\
&q_{12}^+ = mb(b - L_d \cos(\theta_1^+ - \theta_2^+)),\\
&q_{21}^+ = -mbL_d \cos(\theta_1^+ - \theta_2^+), \quad q_{22}^+ = mb^2.
\end{aligned} \tag{11}$$

2.3. *Implementation of the walker*

For each foot and leg, two stops (for the simplest case) are required as shown in Fig. 1. The stops can be made adjustable to allow a range of limiting angles for the foot rotation. Apart from this, contact detection of the foot surface with the stoppers is required in order to start and stop the individual joint actuators between phase transitions. A typical gait of the proposed walker with such stoppers is for 1° slope and 4° toe and heel strike angles.

Apart from stoppers, locking mechanisms are required to lock the ankle joints when the feet are in contact with the stoppers. Locking mechanisms for knee joints are common in kneed bipeds.[11,14] When heel strike is about to occur, the swing foot should be in contact with its heel-side stopper so that the heel of the swing foot touches the ground first at the heel. This lock is released during the heel rocker phase so that when ankle strike occurs, the stance leg is free to rotate about the ankle joint. Toe strike occurs when the toe-side stopper contacts the foot. During the toe rocker phase, there is no need to lock the ankle joint as it is automatically locked due to the self-weight of the biped. However, it needs to be locked during swing phase to ensure that the toe portion of the foot does not scrub the ground. Foot scuffing is ignored in the analysis presented in this paper, since it is possible to avoid foot scuffing by special arrangement of the floor.

3. Passive Dynamic Walking

The proposed walker with symmetric foot ($c = d$) and symmetric toe and heel strike angles (thsa) ($\phi_t = \phi_h$), as shown in Fig. 1 with physical parameters shown in Table I, is considered. Comparison is made with an AR walker of same leg lengths and mass distribution. Substantial increase in speed compared to the AR walker can be observed as shown in Fig. 7. With an increase in toe and heel strike angles, the speed slightly decreases over the range of slopes.

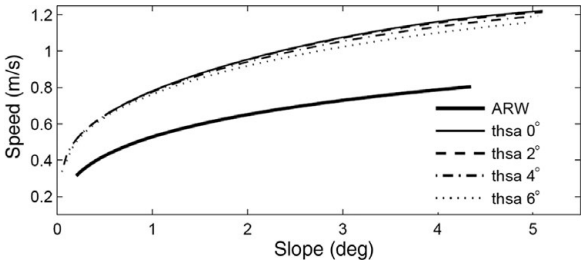


Fig. 7. Speed vs. slope during passive gait.

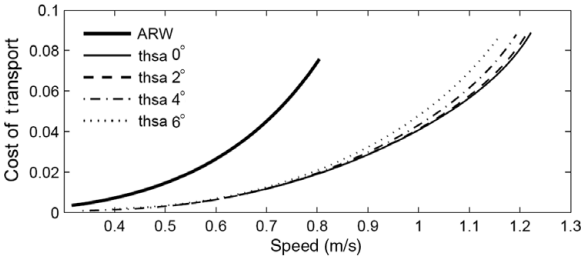


Fig. 8. Cost of transport vs. speed during passive gait.

A measure of energy efficiency in biped walkers is the cost of transport (COT), defined as the energy consumed to move a unit weight through a unit distance.[15,16] Figure 8 shows a comparison of costs of transport for AR walker and HATR walker for various toe and heel strike angles. The proposed walker shows significantly lower cost of transport, especially at higher speeds. Though speed is a general indicator of energy efficiency in passive dynamic walkers, it is not always true as we will see in the later part of the paper where the cost of transport can be different at different slopes but for the same speed.

Stability in the case of dynamic walkers is a measure of how well the walker can tolerate errors in initial conditions or disturbances during walking so that the gait of the walker converges to a limit cycle. For a detailed analysis of various stability measures, refer ref. [17]. In this paper we focus on orbital stability close to the limit cycle. General procedure to evaluate orbital stability is based on the Poincaré return map. This is a linearized form of stability measure determined from the propagation of small perturbations to the limit cycle.

The Poincaré return map is represented as

$$x_{k+1} = \boldsymbol{F}(x_k), \tag{12}$$

where x_k the state vector is defined as

$$x_k = \begin{bmatrix} \theta_1^+[k] \\ \theta_2^+[k] \\ \dot{\theta}_1^+[k] \\ \dot{\theta}_2^+[k] \end{bmatrix}, \tag{13}$$

where θ_1^+ is the active stance leg angle and θ_2^+ is the swing leg angle just after heel strike (when swing leg lifts off the ground). During steady walking,

$$x^* = \boldsymbol{F}(x^*), \tag{14}$$

https://doi.org/10.1017/S0263574711000099 Published online by Cambridge University Press

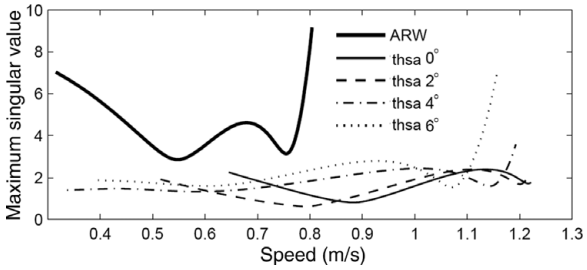


Fig. 9. Maximum singular value vs. speed during passive gait.

where x^* is the equilibrium point. A small perturbation δx_k about the equilibrium point gives

$$\boldsymbol{F}(x^* + \delta x_k) = \boldsymbol{F}(x^*) + \tilde{N}\boldsymbol{F}(x^*)\delta x_k. \tag{15}$$

The eigenvalues of the matrix $\tilde{N}\boldsymbol{F}$ at the equilibrium point indicate whether the equilibrium point is stable. The periodic solutions presented in this paper are all obtained after numerical convergence. Hence, the eigenvalues of the linearized Poincaré map $\tilde{N}\boldsymbol{F}$ lie within unit disc. Maximum singular value of the linearized Poincaré map is a measure of robust stability or convergence rate.[18] For the perturbation δx_k to quickly attenuate, the maximum singular value should be lower. In other words, lower the maximum singular value, higher is the rate of convergence. Since the map is nonlinear, the singular values are determined by numerically linearizing the map about the initial conditions of the limit cycle.

Figure 9 shows a comparison of maximum singular values of the AR walker and the proposed HATR walker for various toe and heel strike angles over a range of speeds. It is clear that the proposed HATR walker is more stable than an AR walker. With a toe and heel strike angle of 4°, feasible walking range extends to lower speeds also. This is a major advantage compared to walkers with zero toe and heel strike angles discussed in refs. [8–10], where lower speeds are not stable. With the proposed walker, higher speeds are possible and that also with higher stability than an AR walker.

The proposed walker with one toe rocker and one heel rocker phase is equivalent to a walker with its foot having two rigid segments joining at the ankle joint. Increasing the total number of foot segments (equally on toe and heel sides with the equivalent foot with rigid segments as shown in Fig. 12) to four shows some interesting results. For the same mass and leg length parameters, and overall foot length but each foot segment half as long as that of previous walker, the walking speed for a range of slopes is shown in Fig. 10. The toe and heel strike angles for all segments are same. At low speeds, the cost of transport is generally very low for dynamic walkers. Hence, a plot of the reciprocal of the cost of transport gives a better indication of efficiency at lower speeds. In order to compare these walkers with same weight, we define efficiency as the distance traveled per unit energy consumed. It can be determined from the cost of transport as

$$\text{Efficiency} = \frac{1}{\text{COT}\,\boldsymbol{x}\,\text{weight}}. \tag{16}$$

At low speeds, the efficiency of the walker is significantly higher than a walker with two-segment feet as shown in

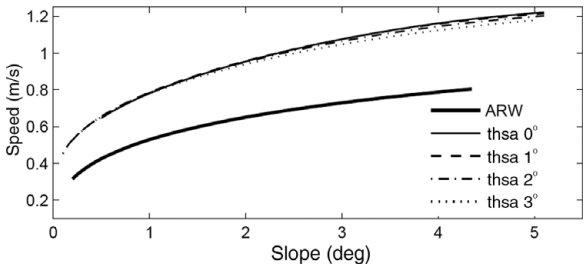


Fig. 10. Speed vs. slope during passive gait of a walker with four-segment foot.

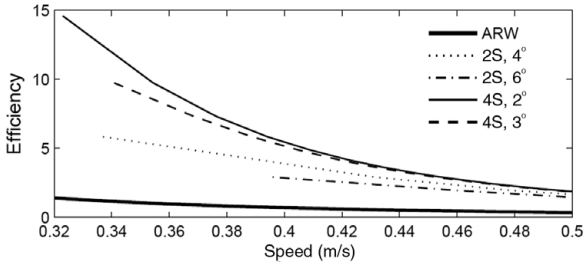


Fig. 11. Efficiency of walkers with two- and four-segment feet at low speed.

Fig. 11. A typical gait of this walker for a slope of 1° with toe and heel strike angle of 3° for each segment.

One possible explanation for the nonexistence of walking cycles at low speeds with flat feet (thsa = 0°) is due to the increase in active leg length during heel and toe rocker phases. With zero toe and heel strike angles, the active leg length during heel and toe rocker phases is always higher than the physical leg length. When the center of gravity of the walker is lifted up due to increased leg length, the potential energy increases and the kinetic energy decreases. The kinetic energy becomes insufficient to lift the center of gravity to the highest point and hence the walker can fall backwards.

4. Energy Losses During Walking

The energy losses for each step during the gait can be divided into those occurring due to impacts within the foot and those occurring due to heel strike (outside the foot). In this section we show that the energy losses because of impacts within the foot can be reduced by increasing the number of foot segments, and the energy losses because of heel-strike impact are dominant at high speeds.

4.1. Losses because of impacts within the foot

Point foot is regarded as an arc foot of zero radius. Similarly, flat foot with heel, ankle, and toe rocker motions, can be regarded as a discretization of arc foot of some radius. This leads to two impacts within the foot, namely, ankle strike (between heel rocker and ankle rocker) and toe strike (between ankle rocker and toe rocker). Heel strike occurs between toe rocker and heel rocker, and involves both legs. Hence, we call it impact occurring outside the foot.

With an increase in the number of impacts occurring within the foot because of an increase in the number of joints in the foot, the energy loss occurring within the foot decreases. The

https://doi.org/10.1017/S0263574711000099 Published online by Cambridge University Press

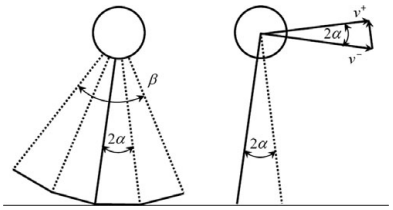


Fig. 12. Segmented arc foot walker.

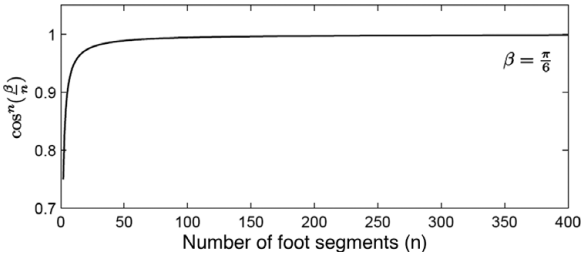


Fig. 13. $\cos^n(\frac{\beta}{n}) = 1$ vs. number of foot segments for $\beta = \pi/6$.

proof of this is given as follows. A similar result for energy loss for n sub-collisions using small angle approximation is given in ref. [19].

For point-foot walker with hip mass alone, the transition equation is given by

$$\dot{\theta}^+ = \dot{\theta}^- \cos 2\alpha, \tag{17}$$

where $\dot{\theta}^-$ and $\dot{\theta}^+$ are the angular velocities of the stance leg before and after the impact, respectively.

If the foot has n segments whose joints lie on an arc of radius equal to the leg length, then the velocity at the end of nth impact is given by

$$\dot{\theta}^{n+} = \dot{\theta}^{1-} \cos^n\left(\frac{\beta}{n}\right), \tag{18}$$

where $\beta = 2n\alpha$ as shown in Fig. 12.

With infinite segments, the segmented foot approaches a smooth arc foot:

$$\lim_{n\to\infty} \cos^n\left(\frac{\beta}{n}\right) = 1, \tag{19}$$

which means there is no loss of kinetic energy throughout the motion on that foot. Again, it follows that if the total loss (where loss is defined as a positive quantity) is zero, each of the individual losses in transitions must be zero.

Figure 13 shows how the fraction in Eq. (18) approaches unity as the number of foot segments approaches infinity, indicating that the final velocity after infinite impacts approaches the initial velocity.

This result still holds when a torque is applied on the stance leg as shown on the right-hand side of Fig. 14. The transitions are assumed to be instantaneous, whereas there exist angular accelerations or decelerations because of the applied torque between the transitions. As the number of segments tends to infinity, the energy loss at each of the transitions tends to zero since

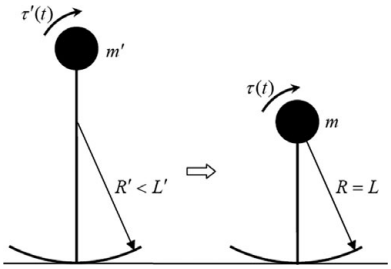


Fig. 14. Equivalence of the general model to the simplest model.

$$\lim_{n\to\infty} \cos\left(\frac{\beta}{n}\right) = 1. \tag{20}$$

Hence, irrespective of the torque applied to the stance leg, the total impact loss tends to be zero as the number of foot segments tends to infinity.

This proof can be extended to more general cases, including slope, leg mass, and applied torque. Let $\boldsymbol{\tau}'(t)$ be the net torque applied to the stance leg of a general biped with arc feet. This torque is the resultant of all the torques because of slope, swing, and stance leg masses, and the hip joint torque. The equation of motion of the stance leg shown on the left-hand side of Fig. 14 is given by

$$m'R'^2\ddot{\theta} = m'g(L'-R')\sin\theta + m'R'(L-R')\dot{\theta}^2\sin\theta + \boldsymbol{\tau}'(t). \tag{21}$$

Multiplying on both sides with $\frac{mR^2}{m'R'^2}$, we get

$$mR^2\ddot{\theta} = \boldsymbol{\tau}(t), \tag{22}$$

where $\boldsymbol{\tau}(t)$ is the arbitrary torque on the simplest model calculated from Eq. (21). Hence, any arc-foot walker with arbitrary arc radius, mass, and leg length parameters can be shown to be equivalent to the simplest model with infinite foot segments and appropriate torque during the rolling phase.

4.2. Losses because of heel strike impact outside the foot

For a given slope, heel-strike energy loss decreases with the increase in foot length for walkers with rigid ankle.[21] This has been found to be so even for the proposed HATR walker with non-zero toe and heel strike angles. However, the advantage of the proposed walker is its ability to walk at lower speeds. The ratio of energy loss because of heel strike per step and the total energy loss per step are close to unity at higher speeds and decreases at lower speeds as shown in Fig. 15. The variation in heel-strike energy loss with respect to toe and heel strike angles is negligible at higher speeds. The total impact energy losses are more or less equally distributed at lower speeds between heel strike loss and the remaining losses, which depend on the number of segments/joints in the foot. This indicates that arc feet, which have zero energy loss during rolling, are highly effective at lower speeds than at higher speeds.

Figure 16 shows the fraction of heel-strike energy loss for four-segment walker. In this case, it can be clearly seen that heel strike loss is dominant and the losses because of impacts within the foot are lowered significantly due to additional

https://doi.org/10.1017/S0263574711000099 Published online by Cambridge University Press

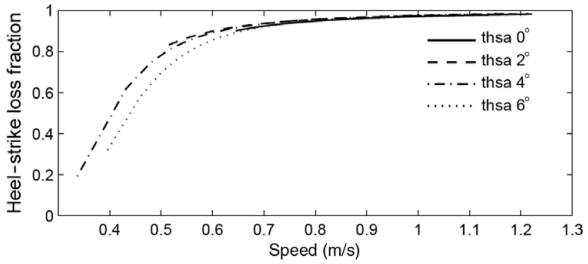


Fig. 15. Fraction of heel-strike energy loss vs. speed for a walker with one toe and one heel.

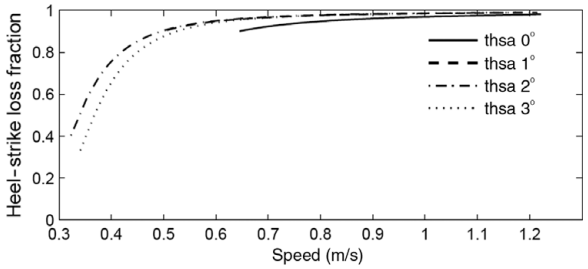


Fig. 16. Fraction of heel-strike energy loss vs. speed for a walker with four-segment foot (two toes and two heels).

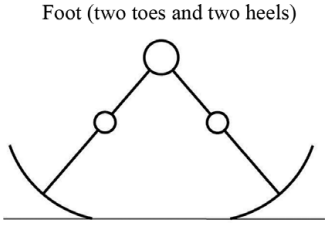


Fig. 17. The proposed walker with infinite foot segments resembling an arc.

segments. However, the overall improvement in the cost of transport is not significant compared to the case of zero toe and heal strike angles (thsa = 0).

The heel-strike energy loss in arc-foot walkers has been shown to decrease with the increase in arc radius up to the leg length.[20] Our walker, however, does not approach arc-foot walking gait even if the number of foot segments is increased to infinity. This is because regardless of the arc radius, rolling till the front tip of the foot and beginning of rolling from the rear tip of the foot occur in the proposed walker as shown in Fig. 17. If this condition is removed, the proposed walker with infinite segments would approach arc-foot walker.

The lowering of cost of transport in the proposed walker lies in the fact that the heel-strike energy loss, which has been found to be a major loss at moderate and higher speeds, is in general a function of deflection angle,[8] with higher leg lengths giving rise to lower deflection angles and hence lower heel-strike energy losses. The deflection angle in the present case is the angle between the active stance leg just prior to heel strike impact and the active stance leg just after heel strike impact. In fact, it is has been shown for simple cases that breaking one impact into a series of impacts reduces the overall impact loss.[19] However, our results in the previous section indicate the contrary for a more realistic case of walker with leg mass. With the introduction of ankle-joint and ankle strike impact, the overall cost of transport increases slightly. While the energy losses inside the foot can be made negligibly small by increasing the number of foot segments, the heel-strike energy loss is independent of the number of segments.

5. Active Walking on Level Ground

The gait of passive dynamic walkers requires very low energy inputs through gravity. One of the straight-forward ways of achieving level ground walking without destroying the passivity property is to imitate walking on a virtual slope.[18,21] This is called virtual gravity approach. In this approach, a virtual gravity field is created on level ground by applying the appropriate control torques. Hence, highly efficient active dynamic walkers can be developed with the associated passivity property by means of minimal control efforts and without disturbing the stability.

In order to imitate a virtual slope of $\boldsymbol{\gamma}_v$ on level ground ($\boldsymbol{\gamma} = 0$), the control input can be determined from[16]

$$\boldsymbol{\tau}_{vg} = \boldsymbol{g}(\boldsymbol{\theta}; 0) - \frac{\boldsymbol{g}(\boldsymbol{\theta}; \boldsymbol{\gamma}_v)}{\cos \boldsymbol{\gamma}_v}. \tag{23}$$

The characteristics of active gait with this control input will exactly be the same as the characteristics of passive gait under acceleration because of gravity of $g/\cos\gamma_v$.

In order to selectively underactuate the walker during toe and heel rocker motions, it is necessary to manipulate the heel, toe, and hip joint torques such that the passivity property is maintained. By underactuation, we denote that any one or more of the actuators (toe, ankle, heel, and hip) is nonoperational during one or more of the phases (toe, ankle, and heel rocker). The constant torque ratio (CTR) formula[13] can be used with zero toe, ankle, or heel torque during toe, ankle, or heel rocker motions, respectively. The energy rate in order to imitate virtual gravity effect is given by

$$\dot{E} = \dot{\boldsymbol{\theta}}^T \boldsymbol{\tau}_{vg}, \tag{24}$$

where E is the total mechanical energy.

Let

$$u_a = \mu u_h, \tag{25}$$

where u_a and u_h are ankle (or toe or heel) and hip torques, respectively, and μ is the constant torque ratio.

The underactuated control torque vector using CTR formula is given by

$$\boldsymbol{\tau}_{uvg} = S u_{uvg} = \begin{bmatrix} \boldsymbol{\mu} + 1 \\ -1 \end{bmatrix} \frac{\dot{E}}{(\boldsymbol{\mu} + 1)\dot{\theta}_1 - \dot{\theta}_2}. \tag{26}$$

In the following sections, we study three different underactuated modes of active walking. Firstly, Section 5.1 outlines the effect of active walking to the ZMP. In Sections 5.2 and 5.3, the walker is fully actuated during the AR phase, but underactuated or not actuated during other phases. In Section 5.4, only hip actuation is present throughout the walking cycle.

https://doi.org/10.1017/S0263574711000099 Published online by Cambridge University Press

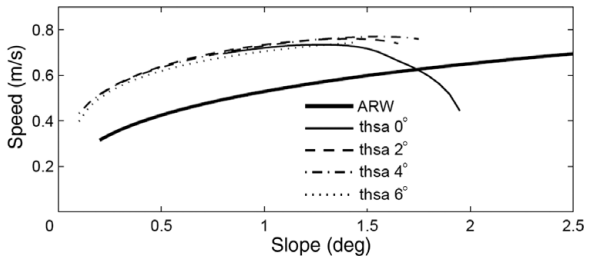


Fig. 18. Speed vs. virtual slope for underactuation during heel and toe rocker.

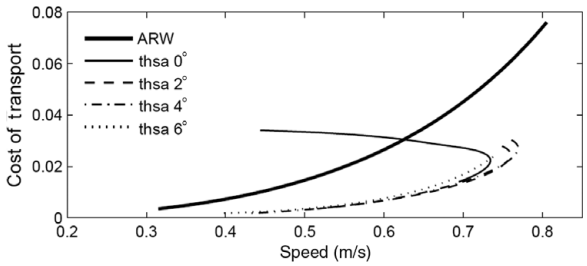


Fig. 19. Costs of transport vs. speed for underactuation during heel and toe rocker.

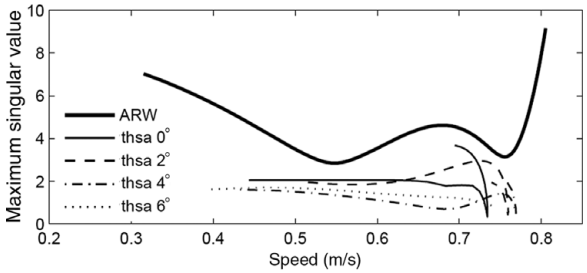


Fig. 20. Maximum singular value vs. speed for underactuation during heel and toe rocker.

5.1. *Zero moment point (ZMP)*

In the case of passive dynamic walking, the ZMP always stays at the pivot point. However, this is no longer true for active walking in a virtual gravity field because of the active torques applied at the pivot points needed for producing the required virtual gravity.

In the case of active walking of dynamic walkers, the ZMP always moves behind the joint in the foot, about which effective stance leg rotates. This results in an unusual design where the toe has to be extended behind the toe joint in order to accommodate the ZMP. Unlike in the present day, AR-only walkers, in which only the heel-side portion of the foot is required for accommodating the ZMP with the toe-side portion functionally unused, the entire foot is utilized for walking in the proposed HATR walker. Both the toe-side and heel-side portions of the foot play a major role in determining the dynamics of the system. For example, see ref. [8] for a parametric study of a flat-foot walker with heel and toe rocker motions.

The distance of the ZMP from the joint (heel, ankle, or toe) depends on the inertia properties of the biped and the torque applied about that joint, which, in turn, depends on the speed of the biped. Therefore, for the walker to be stable, the maximum achievable speed is limited by the length of foot in contact with the ground behind the joint. This fact has to be considered while determining the periodic solutions in active walking.

5.2. *Underactuated mode during toe and heel rocker*

This mode of underactuation can be easily achieved by modifying the existing AR walkers with minimal change in configuration to include toe and heel rocker phases of walking. In this mode of walking, the walker is under actuated only during the toe and heel rocker phases, where hip actuation alone is present. Hence, $\mu = 0$ for the toe and heel rocker motions. For AR motion, $\boldsymbol{\tau}_{vg}$ in Eq. (23) is used.

Figure 18 shows the walking speed obtained for various values of toe and heel strike angles. It can be seen from the figure that higher speeds as compared to AR walker can be achieved in this mode. However, the range of slopes for which feasible solutions exist is smaller as compared to the AR walker. This range further decreases with an increase in toe and heel strike angles. Nevertheless, the costs of transport in this mode are considerably lower than the cost of transport of AR walker as can be seen in Fig. 19. The range of slopes where feasible walking cycles exist is higher for the walker with zero toe and heel strike angles. However, additional range is of little use since the cost of transport is higher and the speed reduces drastically at higher slopes. The maximum singular values of the proposed walker are also lower as shown in Fig. 20, indicating higher local stability. Overall, the results show that more stable and extra efficient walking cycles can be achievable as compared to AR walker with the proposed system at under actuated mode during toe and heel rocker where hip actuation is only present.

5.3. *Unactuated during toe and heel rocker*

The ultimate objective of analyzing different modes is to realize highly efficient and more stable dynamic walkers for design considerations. In an attempt to investigate further the effects to the dynamic walker, a different mode in which none of the actuators are operated during toe and heel rocker phases of walking is considered here. In other words, the dynamics of the walker is completely passive during these two phases. For a stable gait, the maximum achievable speed is limited by the length of foot in contact with the ground behind the joint and the speed of a biped determined by the gravity field control law, which is the function of the virtual slope angle. The maximum virtual slope for the walker at which feasible walking cycle exists can be determined by the ZMP constraint such that the ZMP should stay within the foot area.

Figure 21 shows the obtained walking speeds for the AR walker and the HATR walker for several values of toe and heel strike angles over a range of virtual slopes. As shown in the figure, stable walking cycles exist for this mode of under actuated walking over a broad range of slopes. Particularly at higher toe and heel strike angles, the improvements are clear to achieve higher speeds of the dynamic walker. This result reinforces the potential contribution of the HATR walker design enhancement, as the walker is completely passive during toe and heel rocker phases of walking. For 2° toe and heel strike angles, the speed and the feasible range (as seen in Figs. 22 and 23) are less than those of the AR walker.

https://doi.org/10.1017/S0263574711000099 Published online by Cambridge University Press

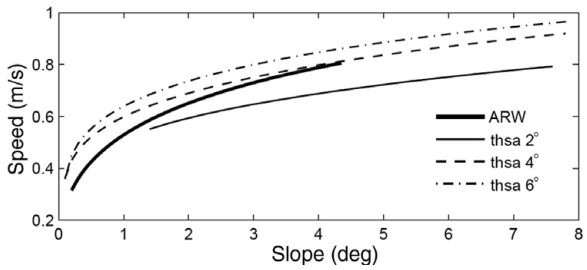


Fig. 21. Speed vs. slope with no actuation during toe and heel rocker.

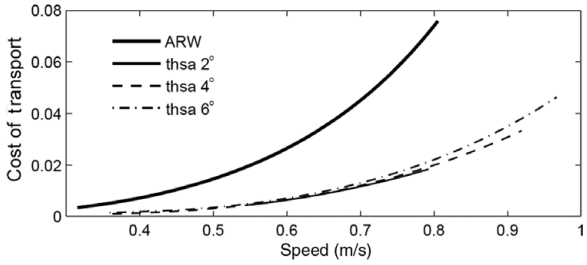


Fig. 22. Cost of transport vs. speed with no actuation during toe and heel rocker.

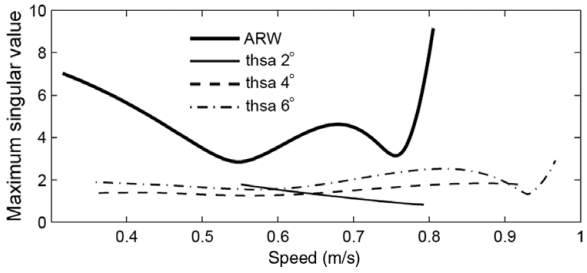


Fig. 23. Maximum singular value vs. speed with no actuation during toe and heel rocker.

Both of these increase with the increase in toe and heel strike angles. No appreciable feasible range of walking speeds has been found for 0° toe and heel strike angles.

Figure 22 shows the associated costs of transport of the walkers. The proposed walker in this mode shows significantly lower cost of transport even at higher speed as compared to the AR walker. As the speed increases, the cost of transport of the proposed HATR walker increases correspondingly to the AR walker but at a much lower rate. The set of results suggests a promising verification for the sole contribution of the system on unactuated modes that the efficiency and the robustness can be improved with the proposed HATR walker for the overall performance.

Figure 23 shows the maximum singular values for various toe and heel strike angles over a range of speeds. It is interesting to note that convergence rate of the proposed walker in this mode is higher as compared to the AR walker over a wide range of speeds even though the walker has completely passive dynamics during toe and heel rocker phases. This indicates, once again, the higher local stability or the disturbance rejection capability for the proposed walker in this mode of walking. Consequently, the plots validate that higher speeds can be achieved through the proposed walker with the higher stability than the one possible in an AR walker. Ultimately, this will bring a major benefit to the proposed dynamic walker's performance in implementation.

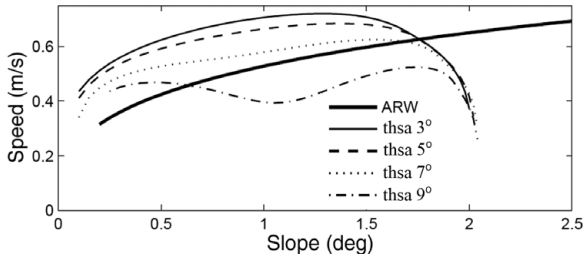


Fig. 24. Speed vs. slope with hip torque alone.

5.4. Hip actuation alone throughout the walking cycle

When toe and heel joints are not actuated, these segments physically will not necessitate actuators at the associated joints. This will bring an added advantage with respect to the number of actuators used in the dynamic walker. As a result, overall weight of the walker can be decreased drastically.

In this mode, the CTR formula in Eq. (26) is used with torque ratio $\mu = 0$ for all the phases of motion. As there are no heel/ankle/toe torques during walking, the situation of ZMP going out of the support region at higher speeds does not arise. This situation is similar to the under actuated virtual passive dynamic walking of an arc-foot walker with hip actuation alone.[22,23]

While it has been reported that it is impossible for an AR walker to walk by hip torque alone with non-zero hip mass,[11] the proposed HATR walker seems to stand as a link between AR walker and arc-foot walker by allowing this mode of actuation. This is particularly interesting because only one actuator (hip) is required for walking. In fact, humans do not use the ankle torque as much as the hip torque.[24,25] This case of underactuation is an important result from biomechanics point of view.

Figure 24 shows the walking speed yet again as a function of virtual slope angles for the AR walker and the HATR walker. The plots indicate that stable walking cycles exist for this mode of under actuated walking over a narrow range of slopes. During this mode of walking, with the smaller virtual slope angles, the attainable speed of the HATR walker is higher than the AR walker over a wide range. However, as the toe and heel strike angle increases, the reachable speed relatively decreases. Nevertheless, the proposed HATR walker presents possible stable walking cycles by hip torque alone. As similar to the previous case, walking cycles do not exist for zero toe and heel strike angles.

Figure 25 demonstrates again the costs of transport for various speeds. Lower costs of transport are obtained at lower virtual slopes. It is interesting to note that, with just a single actuator in this mode of underactuation, the cost of transport significantly lower than that of AR walker can be obtained for considerable range of speeds for certain values of toe and heel strike angles. Figure 26 presents the maximum singular values for various speeds as a measure for local stability and disturbance rejection capability of the dynamic walker. It can be observed from the graph that the maximum singular values of the proposed walker are lower than that of AR walker,

https://doi.org/10.1017/S0263574711000099 Published online by Cambridge University Press

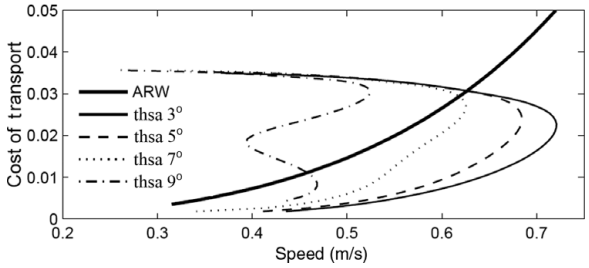


Fig. 25. Cost of transport vs. speed with hip torque alone.

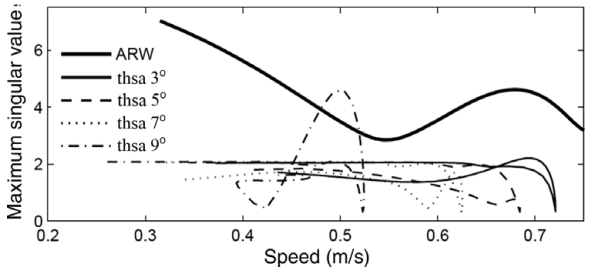


Fig. 26. Maximum singular value vs. speed with hip torque alone.

except at some speeds for higher values of toe and heel strike angles. These plots signify once more the improvements for the proposed walker.

At the same speed, two maximum singular values can be observed in Figs. 20 and 26. However, these do not occur at the same slope. As observed from speed vs. slope plot in Figs. 18 and 24, the speed initially increases with the slope and decreases later. Hence, we find two slopes for the same speed. Since maximum singular value indicates the convergence rate, for the same speed one can choose a virtual slope that gives maximum stability. Similarly, for the same desired speed, one can choose a virtual slope (in Figs. 19 and 25) that gives lower cost of transport.

In conclusion, it is important to note that stable walking cycles are obtainable with this under actuated mode with the proposed HATR dynamic walker by means of only hip actuation. In addition, results reveal significant benefits over AR walker as well.

6. Conclusions

A novel passive dynamic walker with heel, ankle, and toe rocker motions that uses ankle stops to allow heel and toe rocker motions has been proposed. Numerical simulations for a walker with symmetric foot and symmetric toe and heel strike angles show that the walker is more energy-efficient and stable than an AR walker with same leg length and mass distribution. With increase in toe and heel strike angles, the energy efficiency slightly decreases, where as the ability to walk at low speeds increases.

Simulation results show that a walker with four-segment foot improves the efficiency of the walker beyond the efficiency of the walker with two-segment foot at low speeds. A study of energy losses during the gait indicates that the heel-strike energy loss is dominant at higher speeds, whereas energy losses because of impacts occurring within the foot are dominant at lower speeds.

Active walking in three different under actuated modes has been studied, namely, hip actuation during heel/toe rocker, completely passive during heel/toe rocker, and hip actuation alone throughout the walking cycle. For the first two cases, the AR phase uses both ankle and hip joint torques based on virtual gravity. In order to obtain these modes of underactuation, existing AR walkers can be modified to include toe and heel rocker phases of walking with minimal change in configuration.

Hip actuation alone throughout the walking cycle has the advantage of not requiring ZMP constraint for all feasible walking speeds because of lack of heel/ankle/toe joint actuation. This mode of under actuated walking, which is not possible in AR walker, is similar to under actuated walking in arc-foot walkers. Another advantage of such walking is the ability to walk with a single actuator, reducing the overall weight of the walker. Results show that, compared to AR walker, both cost of transport and stability can be higher for this mode of underactuation.

For fully actuated active walking on level ground, the proposed HATR walker requires seven actuators – three for each foot and one at the hip joint. However, we have shown that it is possible to use HATR walker in under actuated mode with either three actuators or just one actuator while retaining significant benefits over AR walker.

Acknowledgments

This work was supported by the National Research Foundation of Korea (NRF) funded by the Ministry of Education, Science and Technology (2010-0029690) and (2008-331-D00027).

References

1. T. McGeer, "Passive dynamic walking," *Int. J. Robot. Res.* **9**(2), 62–82 (1990).
2. A. Goswami, B. Espiau and A. Keramane, "Limit cycles in a passive compass gait biped and passivity-mimicking control laws," *Auton. Robots* **4**(3), 273–286 (1997).
3. D. G. E. Hobbelen and M. Wisse, "Ankle Joints and Flat Feet in Dynamic Walking," *Proceedings of the International Conference on Climbing and Walking Robots (CLAWAR)*, Madrid, Spain (Sep. 22–24, 2004).
4. M. Wisse, D. G. E. Hobbelen, R. J. J. Rotteveel, S. O. Anderson and G. J. Zeglin, "Ankle Springs Instead of Arc-Shaped Feet for Passive Dynamic Walkers," *Proceedings of the IEEE-RAS International Conference on Humanoid Robots*, Genua, Italy (Dec. 2006) pp. 110–116.
5. F. Asano and Z.-W. Luo, "Asymptotically stable biped gait generation based on stability principle of rimless wheel," *Robotica* **27**(6), 949–958 (2009).
6. Y. Harata, F. Asano, Z.-W. Luo, K. Taji and Y. Uno, "Biped gait generation based on parametric excitation by knee-joint actuation," *Robotica* **27**(7), 1063–1073 (2009).
7. P. G. Adamczyk, S. H. Collins and A. D. Kuo, "The advantages of a rolling foot in human walking," *J. Exp. Biol.* **20**(209), 3953–3963 (2006).
8. M. Kwan and M. Hubbard, "Optimal foot shape for a passive dynamic biped," *J. Theor. Biol.* **248**(2), 331–339 (2007).
9. Y. Tazaki and J. Imura, "A study of the energy-saving effect of foot shape on planar passive bipedal walking," *J. Robot. Soc. Japan* **23**(1), 131–138 (2005).
10. J. Kim, C.-H. Choi and M. W. Spong, "Passive Dynamic Walking with Symmetric Fixed Flat Feet," *Proceedings of*

https://doi.org/10.1017/S0263574711000099 Published online by Cambridge University Press

the International Conference on Control and Automation, Guangzhou, China (2007) pp. 24–30.
11. D. G. E. Hobbelen and M. Wisse, "Ankle actuation for limit cycle walkers," *Int. J. Robot. Res.* **27**(6), 709–735 (2008).
12. R. P. Kumar, J. W. Yoon, Christiand, and G. Kim, "The simplest passive dynamic walking model with toed feet: A parametric study," *Robotica* **27**(5), 701–713 (2009).
13. F. Asano, Z.-W. Luo and M. Yamakita, "Biped gait generation and control based on a unified property of passive dynamic walking," *IEEE Trans. Robot. Autom.* **21**(4), 754–762 (2005).
14. S. H. Collins, M. Wisse and A. Ruina, "A three-dimensional passive-dynamic walking robot with two legs and knees," *Int. J. Robot. Res.* **20**(7), 607–615 (2001).
15. S. Collins, A. Ruina, R. Tedrake and M. Wisse, "Efficient bipedal robots based on passive-dynamic walkers," *Science* **307**, 1082–1085 (2005).
16. A. D. Kuo, "Choosing your steps carefully: Trade-offs between economy and versatility in dynamic walking bipedal robots," *IEEE Robot. Autom. Mag.***14**(2), 18–29 (2007).
17. D. G. E. Hobbelen and M. Wisse, "A disturbance rejection measure for limit cycle walkers: The gait sensitivity norm," *IEEE Trans. Robot. Autom.* **23**(6), 1213–1224 (2007).
18. F. Asano, M. Yamakita, N. Kamamichi and Z.-W. Luo, "A novel gait generation for biped walking robots based on mechanical energy constraint," *IEEE Trans. Robot. Autom.* **20**(3), 565–573 (2004).
19. A. Ruina, J. E. A. Bertram and M. Srinivasan, "A collisional model of the energetic cost of support work qualitatively explains leg sequencing in walking and galloping, pseudo-elastic leg behavior in running and the walk-to-run transition," *J. Theor. Biol.* **237**(2), 170–192 (2005).
20. F. Asano and Z.-W. Luo, "The Effect of Semicircular Feet on Energy Dissipation by Heel-Strike in Dynamic Bipedal Walking," *Proceedings of the IEEE International Conference on Robotics and Automation* (ICRA), Roma, Italy (April 2007) pp. 3976–3981.
21. M. W. Spong, "Passivity-Based Control of the Compass Gait Biped." *Proceedings of the 14th World Congress IFAC* (1999) pp. 19–23.
22. F. Asano and Z.-W. Luo, "On Energy-Efficient and High-Speed Dynamic Biped Locomotion with Semicircular Feet," *Proceedings of the IEEE/RSJ International Conference on Intelligence Robots Systems,* Beijing, China (Oct. 9–15, 2006) pp. 5901–5906.
23. F. Asano and Z.-W. Luo, "Dynamic Analyses of Under actuated Virtual Passive Dynamic Walking," *Proceedings of the IEEE International Conference on Robotics and Automation* (ICRA), Roma, Italy (April 2007) pp. 3210–3217.
24. A. D. Kuo and F. E. Zajac, "A biomechanical analysis of muscle strength as a limiting factor in standing posture," *J. Biomech.* **26**(1), 137–150 (1993).
25. K. Y. Yi and Y. F. Zheng, "Biped locomotion by reduced ankle power," *Auton. Robots* **4**, 307–314 (1997).

https://doi.org/10.1017/S0263574711000099 Published online by Cambridge University Press